Dynamic Density Functional Study on the Structure of Thin Polymer Blend Films with a Free Surface

Hiroshi Morita,*,† Toshihiro Kawakatsu,‡ and Masao Doi‡

Japan Chemical Innovation Institute, Research & Education Center, Nagoya University, Furo-cho, Chikusa-ku, Nagoya, 464-8601 Japan; and Department of Computational Science and Engineering, Graduate School of Engineering, Nagoya University, Furo-cho, Chikusa-ku, Nagoya, 464-8603 Japan

Received February 26, 2001; Revised Manuscript Received August 27, 2001

ABSTRACT: Using the dynamic density functional method, we studied the structural evolution of a thin film of polymer blends placed between the solid substrate and free surface. We observed various types of structural instabilities such as the spinodal wave and the roughening of the free surface due to droplet formation. We proposed a simple theoretical argument based on the Neumann triangle condition among the interfacial tensions to construct a phase diagram for the instability of the free surface and confirmed this by a series of dynamic density functional simulations.

1. Introduction

Thin films of polymer blends play important roles in various industrial applications, such as coating of solid surfaces, production of photo resists, controlling adhesions and biological separations, etc. If one of the two surfaces of the film is faced to the air or to a liquid solvent, this surface should be regarded as a free surface. In such a case, the roughening transition of the surface can take place as a result of the phase separation around the surface. As the transparency of the film is largely determined by the roughness of the free surface, controlling the surface roughening is very important in the applications of the polymer films to photo resist[1] and related optical devices.

Many experimental techniques have been used to study the surface structures and the inner structures of thin films of polymer blends. Tanaka et al. studied the surface of ultrathin films of a PS/PVME mixture using atomic force microscopy (AFM) and observed a formation of droplets at the free surface.[2,3] A similar undulation of the free surface was also reported by Karim et al. for the thin films of the dPS/PVME mixture.[4] Another class of useful experimental techniques is the secondary ion mass spectroscopy (SIMS) and the nuclear reaction analysis (NRA) etc., with which one can measure the "depth profile", i.e., the density distribution of each component in the direction perpendicular to the surface of the film. Krausch et al.[5] and Geoghegan et al.[6] studied the temporal change of the depth profiles during the annealing process of thin films of the dPEP/PEP and the dPS/PαMS mixtures, respectively. Both of them observed a growth of phase separated region which starts from the free surface and the substrate wall and then propagates toward the center of the film. They called this growth mode the "spinodal wave".

Computer simulations were also applied to study the structural evolution of thin films of polymer blends mainly with the use of the time dependent Ginzburg−Landau (TDGL) model for homogeneous surface[7,8] and for patterned inhomogeneous surface.[9,10] Brown and Chakrabarti[7] and Puri and Frisch[8] simulated the dynamics of the phase-separation of a binary mixture near a substrate wall using the 2-dimensional TDGL model, where the effect of the wall was introduced through "a wall potential" in the free energy functional. Krausch et al.[5] have simulated a thin film of a binary mixture placed between two solid walls and observed the propagation of phase boundaries similar to the experimentally observed "spinodal wave". Kielhorn and Muthukumar[9] and Karim et al.[10] used a similar model for the simulations of a film on a patterned substrate that controls the phase separation near the wall. These studies have shown that the TDGL model can reproduce the experimental observation for the phase separation in thin films of polymer blends.

In the present study, we simulate the dynamics of the phase separation and the roughening transition of the free surface of thin films composed of binary homopolymer blends using the dynamic density functional method (DDF).[11−13] The DDF method was originally proposed by Fraaije[11] and was applied to many dynamical phenomena of polymer mixtures, such as polymer adsorption onto a solid surface from a polymer solution,[12] microphase separation of block copolymer systems,[13] etc. The advantage of the DDF method is that the architectures of the component polymer chains are taken into account through the path integral method. The path integral method has been applied to the equilibrium structure of thin films of block copolymers by Matsen[14] and by Pickett and Balazs.[15] In this paper, as we are interested in the structural evolution, we will use the dynamic extension of the method.

This paper is organized as follows. In section 2, we describe our simulation method for the phase separation of thin polymer blend films with a free surface and a substrate wall. In section 3, we show the simulation results on the depth profiles and the surface structures. In section 4, we propose a simple model for the surface roughening conditions and derive the phase diagrams for the surface structures. These theoretical predictions are verified in section 5 using the DDF simulations. In section 6, the relationship between our results and previous experimental results is discussed.

* To whom correspondence should be addressed.
† Research & Education Center, Nagoya University.
‡ Graduate School of Engineering, Nagoya University.

10.1021/ma010346+ CCC: $20.00
Published on Web 11/02/2001

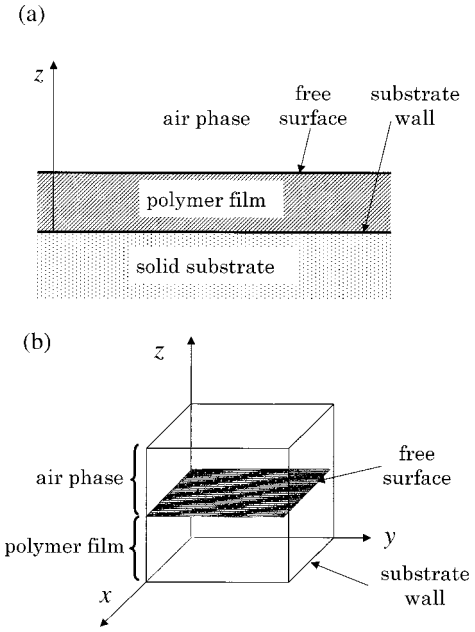

Figure 1. Schematic pictures of (a) the system under consideration and (b) the simulation system, respectively.

2. Method of the Simulation

The system we study is shown in Figure 1: a thin film of an A/B polymer blend is placed on a solid substrate. Above the film is air and the boundary between the air phase and the polymer film corresponds to a free surface that is expected to show shape instabilities.

To simulate such a system, we adopt the DDF method[11−13] that can trace the dynamical process of the phase separation. The advantage of the DDF method is the wide applicability to various types of polymer architectures such as block copolymers, branched polymers, or more complicated polymers. As a first step, we here study thin films composed of a blend of homopolymers.

Let $\phi_A(\mathbf{r},t)$ and $\phi_B(\mathbf{r},t)$ be the segment density of polymers A and B at position $\mathbf{r}$ and time t. In the DDF method, the dynamics of the system is modeled by the Cahn−Hilliard type equation for the segment density fields $\phi_A(\mathbf{r},t)$ and $\phi_B(\mathbf{r},t)$:

$$\frac{\partial}{\partial t}\phi_K(\mathbf{r},t) = L_K\nabla^2\frac{\delta F}{\delta\phi_K(\mathbf{r})}\bigg|_{\phi_K(\mathbf{r})=\phi_K(\mathbf{r},t)} \tag{1}$$

where K is the index for the segment type (A and B in the present binary blend case), L_K is the mobility coefficients, and $F = F[\{\phi_K(\mathbf{r})\}]$ is the free energy functional of the system. The functional derivative $\{\delta F\}/\{\delta\phi_K(\mathbf{r})\}$ represents the chemical potential of the polymer segment K at the position $\mathbf{r}$. Note that there are no chain-level dynamics in this model, and our dynamic equation, eq 1, corresponds neither to the Rouse dynamics nor to the reptation dynamics. However, eq 1 guarantees that the local segment motion is driven in the direction where the total free energy is reduced. Such a process retains the essential aspects of the diffusion dynamics of phase-separating polymer systems on the coarse-grained level. In this case, the mobility coefficient L_K should be identified with the diffusion constant for the collective motion rather than the diffusion constant of a single segment.

Though the system described by eq 1 is not in equilibrium, the chemical potential $\{\delta F\}/\{\delta\phi_K(\mathbf{r})\}$ can be calculated by using the equilibrium statistical mechanics using the following trick. If there is an external field $U_K(\mathbf{r})$ acting on the K-type segment, the chemical potential for the K-type segment becomes equal to $\{\delta F\}/\{\delta\phi_K(\mathbf{r})\} + U_K(\mathbf{r})$. Suppose that we apply a hypothetical external field $U_K(\mathbf{r}) = -\{\delta F\}/\{\delta\phi_K(\mathbf{r})\}$, which exactly cancels the current chemical potential, then the system should be in equilibrium. Therefore $\{\delta F\}/\{\delta\phi_K(\mathbf{r})\}$ can be obtained by asking what is the external field that makes the current density profile $\phi_K(\mathbf{r},t)$ the equilibrium one.

This is done by using the path integral method and the mean field approximation. Consider a K-type chain placed in a potential field $V_K(\mathbf{r})$. Let $Q_K(i,\mathbf{r}_i;j,\mathbf{r}_j)$ be the statistical weight of the subchain between ith and jth segments that are fixed at positions $\mathbf{r}_i$ and $\mathbf{r}_j$, respectively. This is obtained by solving the following Edwards equation[16−18]

$$\frac{\partial}{\partial i}Q_K(0,\mathbf{r}_0;i,\mathbf{r}) = \left[\frac{b^2}{6}\nabla^2 - \beta V_K(\mathbf{r})\right]Q_K(0,\mathbf{r}_0;i,\mathbf{r}) \tag{2}$$

where $\beta = 1/(k_BT)$, and b is the Kuhn statistical length. The initial condition for $Q_K(i,\mathbf{r}_i;j,\mathbf{r}_j)$ is

$$Q_K(0,\mathbf{r}_0;i=0,\mathbf{r}) = \delta(\mathbf{r}-\mathbf{r}_0) \tag{3}$$

Given $Q_K(i,\mathbf{r}_i;j,\mathbf{r}_j)$, the segment density of K-type at position $\mathbf{r}$ can be obtained as

$$\phi_K(\mathbf{r}) = n_K\int_0^{N_K} di\frac{\int d\mathbf{r}_0\int d\mathbf{r}_{N_K}Q_K(0,\mathbf{r}_0;i,\mathbf{r})Q_K(i,\mathbf{r};N_K,\mathbf{r}_{N_K})}{\int d\mathbf{r}_0\int d\mathbf{r}_{N_K}Q_K(0,\mathbf{r}_0;N_K,\mathbf{r}_{N_K})} \tag{4}$$

where n_K is the total number of the K-type polymer chains in the system, and N_K is the total number of the segments in the K-type polymer chain.

Now in the mean field approximation, the potential field $V_K(\mathbf{r})$ can be regarded as a sum of the mean field created by the surrounding segments and the external field $U_K(\mathbf{r})$. Hence $V_K(\mathbf{r})$ is given by

$$V_K(\mathbf{r}) = \sum_{K'}\chi_{KK'}\phi_{K'}(\mathbf{r}) + U_K(\mathbf{r}) \tag{5}$$

where $\chi_{KK'}$ is the χ parameter which stands for the interaction between the K-type segment and the K′-type segment. For given density profile $\{\phi_K(\mathbf{r},t)\}$, we solve the set of eqs 2−5 to obtain the chemical potential $-U_K(\mathbf{r},t)$ for the current density profile $\{\phi_K(\mathbf{r},t)\}$.

For the system shown in Figure 1, we have to add the effect of the substrate and the free surface. The effect of the substrate can be taken into account by adding the wall potential $P_K(\mathbf{r})$,[7] which acts for the segment contacting with the substrate wall, and can be written as

$$P_K(\mathbf{r}) = \chi_{KS}bk_BTf(z) \tag{6}$$

where χ_{KS} measures the strength of the interaction between the polymer segment K and the substrate (hereafter, we call this as "surface χ parameter") and $f(z)$ is a rapidly decaying exponential function that satisfies $\int_0^\infty f(z)\,dz = 1$ with decay length ξ. The potential $V_K(\mathbf{r})$ is now given by

$$V_K(\mathbf{r}) = \sum_{K'}\chi_{KK'}\phi_{K'}(\mathbf{r}) + U_K(\mathbf{r}) + P_K(\mathbf{r}) \tag{7}$$

The effect of the free surface can be taken into account by explicitly considering the void component in the system.[19,20] The "void" represents the air, and is treated as the solvent in the standard path-integral calculation for polymer solution. Therefore, the void V is assumed to have the same volume as the polymer segment, and its interaction with the polymer is specified by the χ parameters χ_{AV} and χ_{BV}, where χ_{AV} and χ_{BV} are taken to be large since polymers cannot diffuse into the air. In practice, we cannot make the polymer concentration in the air phase zero, but we chose the χ parameters so that the polymer segment in the air phase becomes less than 1%.

In solving the Edwards equation, eq 2, boundary conditions are needed. For the four boundaries perpendicular to the substrate wall, the periodic boundary conditions are used. At the boundary on the substrate wall, the Dirichlet condition Q

$= 0$ is used, since the polymer chains cannot cross the boundary.[21] At the top wall of the simulation box, the Neumann condition $\partial Q/\partial z = 0$ is used to minimize the finite size effect of the simulation box.

In solving the diffusion equation, eq 1, the same boundary conditions as for Q are used except for that at the substrate wall, where the boundary condition is that the segment flux perpendicular to the wall vanishes.

3. Simulations on the Structural Formations at the Free Surface

We used a cubic simulation box that is divided into $64 \times 64 \times 64$ cubic meshes with size b, each of which is occupied either by the A segment, the B segment, or the "void". The decay length and the surface χ parameters in eq 6 are chosen as $\xi = 1.0$, $\chi_{AS} = -1.0$ and $\chi_{BS} = -0.9$, respectively. The negative signs of the surface χ parameters mean that the polymers are attracted to the substrate wall.

Both A and B chains are assumed to be homopolymers composed of five segments. To simulate the phase separation in the thin film, we need an appropriate set of χ parameters so that the system separates into three phases, i.e., the A-rich, the B-rich, and the void-rich phases. To fulfill this requirement, we chose the χ parameters as $\chi_{AB} = 1.0$, $\chi_{AV} = 2.0$, and $\chi_{BV} = 1.8$, which are determined using the free energy expression of the Flory−Huggins theory.

$$F_{FH} = \frac{\phi_A}{N_A}\ln \phi_A + \frac{\phi_B}{N_B}\ln \phi_B + \phi_V \ln \phi_V + \chi_{AB}\phi_A\phi_B + \chi_{AV}\phi_A\phi_V + \chi_{BV}\phi_B\phi_V \quad (8)$$

The initial state of our simulation consists of two phases: one is the void-rich phase (air phase) in the upper region of the simulation box, and the other is a uniformly mixed A/B polymer blend (polymer film) close to the substrate wall. Due to the boundary conditions we assumed, the total amounts of each species are conserved. The initial volume fractions of the polymer A, the polymer B, and the void are chosen to be 0.25, 0.25, and 0.5. For the equation of motion, eq 1, we assume $L_K = 1.0$ for all segments, and eq 1 is integrated numerically using the Euler method with $\Delta t = 0.05$. Althogh L_K for the solvent, in general, should be much larger than the L_K for the polymers A and B, we used the same value for all species for the sake of the computational convenience, rather than including some intrinsic physics associated with the polymeric nature of the system.

Figure 2 shows the time evolution of the segment distributions in the film, where red and blue regions correspond to the high and low density regions, respectively. It is observed that the film typically consists of three types of domains. One is the layered domain near the substrate wall, the other is the domain near the free surface, and the third is the disordered domains in the middle of the film.

In Figure 3, we show the temporal evolution of the depth profiles of the segment densities. In this figure, the segment densities are averaged in the $x-y$ plane parallel to the substrate wall. In the region $z > 40.0$, the densities of the polymers A and B are nearly zero, which means that the present model can appropriately describe the air phase. Near the substrate wall and near the free surface, we see distinctive peaks that correspond to the layered domains shown in Figure 2. The peaks become less pronounced in the middle of the film. The flat density profile in the middle does not mean that the phase separation is delayed in the middle. Rather it is an artifact due to the averaging of the randomly oriented domains. As it is seen in Figure 2, phase separation takes place uniformly in the film, but the

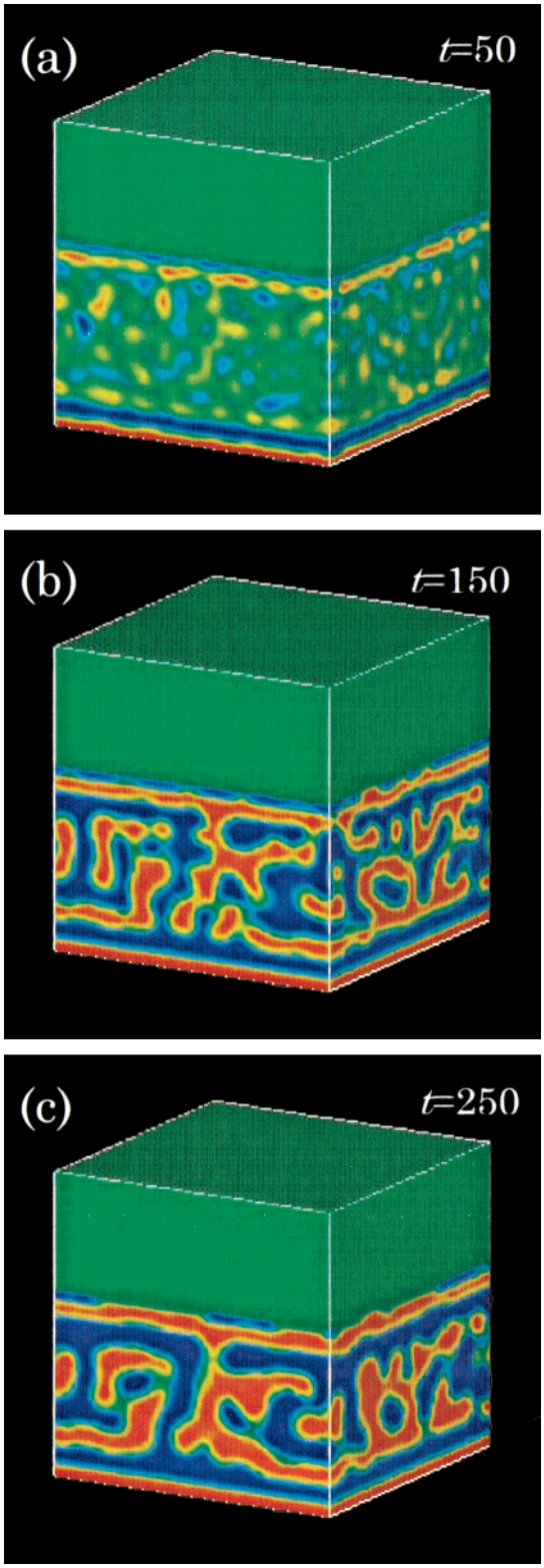

Figure 2. 3D images of the calculated domain structures of the phase separation between polymers A and B. Parts a−c show the density differences $\phi_A(\mathbf{r}) - \phi_B(\mathbf{r})$ calculated for the times $t = 50$, 150, and 250, respectively. Red and blue regions show the regions where $\phi_A(\mathbf{r}) - \phi_B(\mathbf{r})$ takes high and low values, respectively.

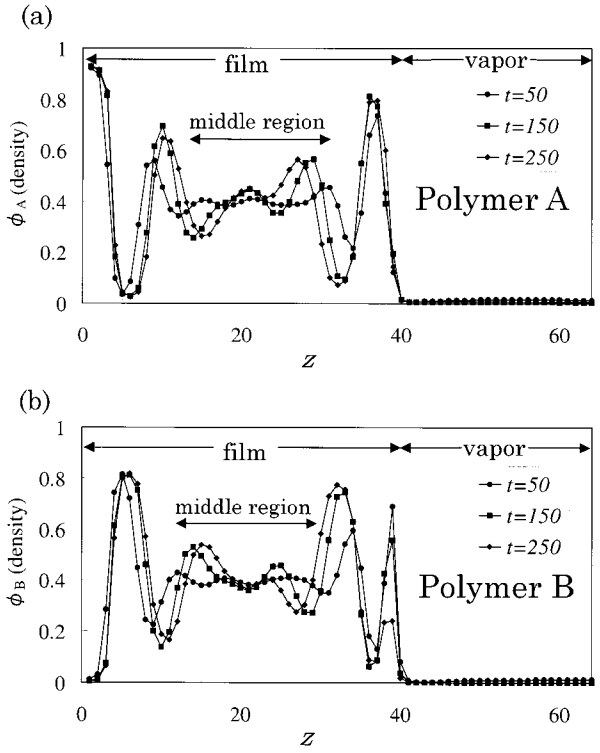

Figure 3. Depth profiles of (a) the polymer A and (b) the polymer B, respectively. Horizontal *z*-axis indicates the distance from the substrate wall.

averaging in the $x-y$ plane for the randomly oriented domains in the middle gives the flat profile in Figure 3. Notice that as time goes on the fronts of the phase separated regions propagate toward the middle region from both sides of the film. This front propagation has been seen in experiments,[5,6] and called the spinodal wave. Our simulation indicates that the mechanism of the spinodal wave is the gradual reorientation of the domains.

Figure 4 shows the time evolution of the shape of the free surface that is defined as the surface where the density of the void takes the half values of its maximum value. During $t = 50-150$, the free surface is almost flat. Around $t = 200$, however, the free surface starts to roughen. In Figure 4f, we show the domain boundaries on the plane of the initial free surface, the plane of $z = 39$. Many holes and islands (or droplets) at the free surface are observed. We notice from Figure 3 that this roughening transition is accompanied by the diffusion of the polymer B from the free surface to the bulk of the film. The roughening transition of the free surface is coupled with the domain growth inside the film.

Our simulation indicates that there are two factors for the surface roughening. One is the volume fraction of the minor phase at the free surface (B-phase in the present case), and the other is the interfacial tension that stabilizes the droplets. In the next section, we discuss the role of the interfacial tension using a simple analytical model.

4. Analysis of the Surface Roughening by a Simple Model

In the previous experimental studies,[2-4] the roughening of the free surface is attributed to the formation of droplets. The result shown in Figure 2 agrees with this experimental finding. Here, we propose a simple model to describe such phenomena.

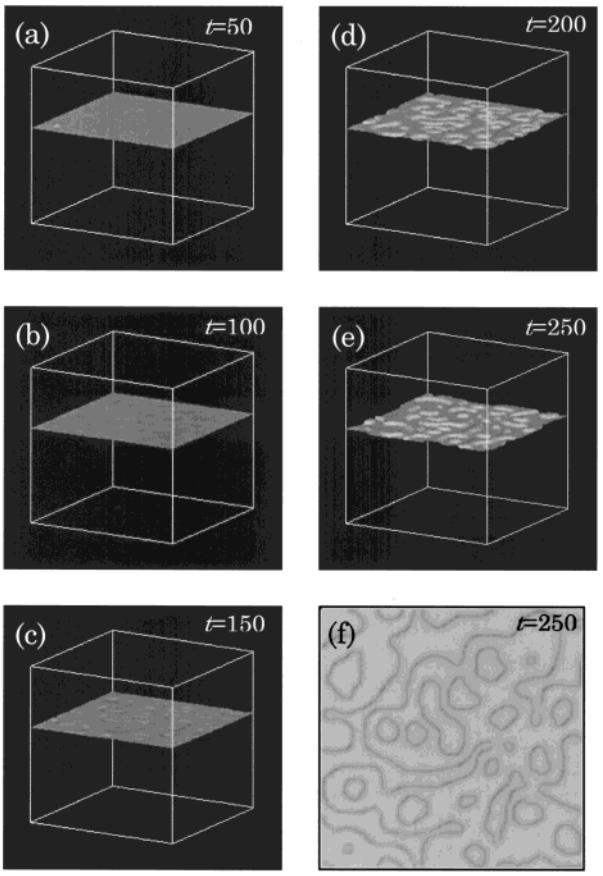

Figure 4. Calculated interfacial structures between the polymer film and the void phase. Parts a−e show the structures at the time $t = 50$, 100, 150, 200, and 250, respectively. Part f shows the domain boundaries on the plane $z = 39$ (the free surface) at $t = 250$.

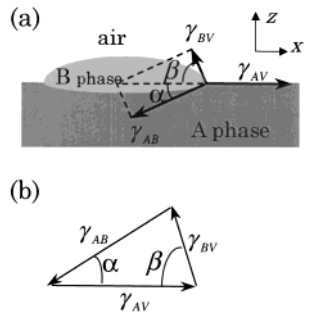

Figure 5. Model for the Neumann triangle condition at the interface among the polymers A, B, and the void phases. This shows the equilibrium force balance among the interfacial tensions, γ_{AB}, γ_{AV}, and γ_{BV}. Definitions of the angles α and β are also shown in this figure.

As is shown in Figure 5a, consider the situation that a droplet of phase B (the polymer B rich phase) exists at the interface between the phase A (the polymer A rich phase) and phase V (the air). The condition for the three phases to meet at a point is that the three interfacial tensions γ_{AB}, γ_{AV}, and γ_{BV} between the phases can form a triangle, called the Neumann triangle shown in Figure 5b.[22] This condition is written as

$$(\gamma_{AB} + \gamma_{BV}) - \gamma_{AV} > 0, \tag{9}$$

$$(\gamma_{AV} + \gamma_{BV}) - \gamma_{AB} > 0, \tag{10}$$

and

$$(\gamma_{AB} + \gamma_{AV}) - \gamma_{BV} > 0. \quad (11)$$

What will happen when one of these conditions is not satisfied can be inferred from the change of the shape of the Neumann triangle. For example, consider what will happen when $(\gamma_{AB} + \gamma_{AV}) - \gamma_{BV}$ becomes negative. When $(\gamma_{AB} + \gamma_{AV}) - \gamma_{BV}$ is positive but close to 0, the Neumann triangle construction indicates that most of the droplet of B is immersed in A phase. Therefore, when $(\gamma_{AB} + \gamma_{AV}) - \gamma_{BV}$ becomes negative, the droplet B will be included in the A phase. Table 1 summarizes the results of such reasoning. In case I, a droplet is embedded inside the film. In cases II and III, droplet of B exists on the surface. This situation is further classified into the two cases, the lower convex case II where α is larger than β, and the upper convex case III where α is less than β. Such classification is done since the free surface becomes rougher in the upper convex case than in the lower convex case. Cases II and III are distinguished according to whether

$$\gamma_{AB} - \gamma_{BV} > 0 \quad (12)$$

is satisfied or not. In case IV, a complete wetting layer of the B phase covers the A phase. Case V corresponds to an isolated B droplet that is separated from the A phase, and should not be observed in real system due to the effect of gravity.

The Neumann triangle conditions, eqs 9−11 and eq 12, can be rewritten in a more useful form in terms of the Flory's interaction parameters χ_{KK}'s and the numbers of segments per chain N_K's. Assuming a hyperbolic-tangent type interfacial profile in the Flory−Huggins free energy, Broseta et al.[23] derived the following approximate formula for the interfacial tension

$$\gamma_{AB} = \frac{k_B T}{b^2}\left[\frac{\chi_{AB}}{6}\right]^{1/2}\left[1 - \frac{\pi^2}{12\chi_{AB}}\left[\frac{1}{N_A} + \frac{1}{N_B}\right]\right] \quad (13)$$

Here, the origin of the terms with $1/N$-dependence is the translational entropy of the chains. As we assumed that the void has the same size as the polymer segment, we obtain similar formulas to estimate γ_{AV} and γ_{BV}:

$$\gamma_{AV} = \frac{k_B T}{b^2}\left[\frac{\chi_{AV}}{6}\right]^{1/2}\left[1 - \frac{\pi^2}{12\chi_{AV}}\left[\frac{1}{N_A} + 1\right]\right] \quad (14)$$

$$\gamma_{BV} = \frac{k_B T}{b^2}\left[\frac{\chi_{BV}}{6}\right]^{1/2}\left[1 - \frac{\pi^2}{12\chi_{BV}}\left[1 + \frac{1}{N_B}\right]\right], \quad (15)$$

By substituting eqs 13−15 into each of the equations in Table 1, the phase diagram for the free surface structure can be obtained. Equations 13−15 contain five parameters, i.e. χ_{AB}, χ_{AV}, χ_{BV}, N_A, and N_B. By fixing N_A, N_B, and χ_{AV} as $N_A = N_B = 5$, and $\chi_{AV} = 2.0$, we can obtain a phase diagram as a function of χ_{AB} and χ_{BV}. Figure 6 shows such a phase diagram. Starting from the point indicated by the open circle, increasing the value of χ_{AB} changes the structure from II to III, and the surface roughness increases.

A similar phase diagram for the case of $N_A = N_B = 5$ and $\chi_{AB} = 1.3$ is shown in Figure 7, where only the lower triangular part of the phase diagram is shown since the diagram is symmetric with respect to the line of $\chi_{AV} = \chi_{BV}$. Starting from the state in the complete wetting region IV, an increase in the value of χ_{BV} changes the structure to the partial wetting case (II or III) so that the total area of the interface between the B and the void phases is reduced.

It should be noted that, in addition to the five parameters used in the construction of these phase diagrams, there are other important parameters, such as the volume fraction of the component that forms droplets at the surface. The surface instability due to the chain conformation[24] may be concerned with this droplet formation. These effects will be discussed in a forthcoming paper.[25]

As the procedure for constructing the phase diagrams described in this section is easy to perform, this analyti-

Table 1. Conditions of Inequality of Interfacial Tension for Each Structures[a]

	eq.(9) $(\gamma_{AB}+\gamma_{BV})-\gamma_{AV}$	eq.(10) $(\gamma_{AV}+\gamma_{BV})-\gamma_{AB}$	eq.(11) $(\gamma_{AB}+\gamma_{AV})-\gamma_{BV}$	eq.(12) $\gamma_{AB}-\gamma_{BV}$
(I)	+	+	−	−
(II)	+	+	+	−
(III)	+	+	+	+
(IV)	−	+	+	+
(V)	+	−	+	+

[a] + and − mean the positive and negative values of the formulas in the first line of this table, respectively.

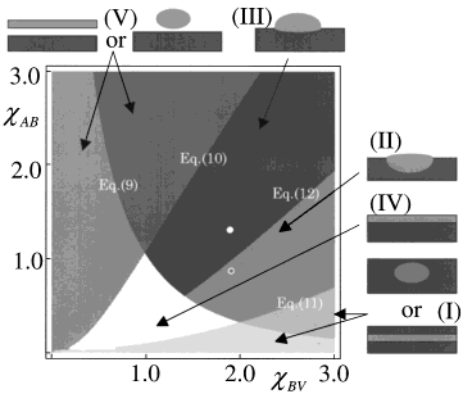

Figure 6. Phase diagram for the surface roughening in the case of $N_A = N_B = 5$ and $\chi_{AV} = 2.0$. The schematic pictures of the structures I−V shown in Table 1 are also indicated. The boundaries between the phases are obtained using eqs 9−12. Solid and open circles correspond to the points where the simulations are performed.

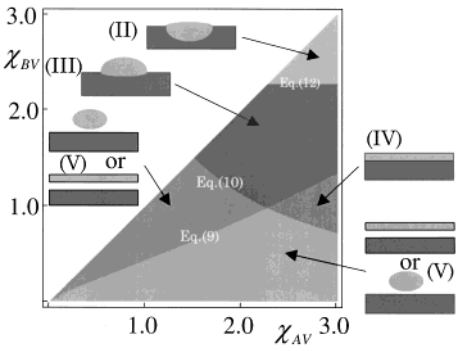

Figure 7. Phase diagram for the surface roughening in the case of $N_A = N_B = 5$ and $\chi_{AB} = 1.3$. The schematic pictures of the structures II − V shown in Table 1 are also indicated. The boundaries between the phases are obtained using eqs 9, 10, and 12.

Table 2. χ Parameters for the DDF Calculations

	χ_{AB}	χ_{AV}	χ_{BV}
case II	0.8	2.0	1.9
case III	1.3	2.0	1.9
case IV	0.5	2.25	1.75

cal method will be a useful tool in predicting the structures of the free surface. In the next section, we perform DDF simulations to check the validity of this method.

5. Comparison between the Theoretical Results and the DDF Simulations

5.1. Validation of the Theoretical Phase Diagrams. To verify the phase diagrams shown in Figures 6 and 7, we performed three types of simulations for the cases II, III, and IV in Table 1. The simulation system is a cubic box with $32 \times 32 \times 32$ spatial meshes and with the same types of boundary conditions as those in section 3. The chain lengths of the polymers A and B are $N_A = N_B = 5$. The parameters of the wall potential are chosen as $\xi = 0.0$ (i.e., $f(z) = \delta(z)$), $\chi_{AS} = -0.5$, and $\chi_{BS} = -0.25$, respectively. The values of the other χ parameters used in these simulations are shown in Table 2. Cases II and III are also shown in Figure 6 by the solid circle and the open circle, respectively. (Case IV is not shown in the phase diagrams.)

As the initial condition for the simulations, we selected a phase separated structure for the polymer film, in which the A polymer is localized near the substrate wall and the B polymer near the free surface. The thickness of the film is set to be $6b$, and the total composition of the polymer film is taken to be A:B = 4:1. Due to this asymmetric initial condition and the asymmetric choice of the χ parameters mentioned before, the B polymer is expected to form minority domains at the free surface.

To solve the equation of motion, we assumed that the parameters Δt and L_K are the same as those in section 3. Figure 8, parts a−c, d−f, and g−i, shows the simulation results at $t = 2500$ for the cases II (lower convex), III (upper convex), and IV (complete wetting), respectively. In each column, the left side, the center, and the right side figures show the boundary surfaces of the A-polymer rich domains, the B-polymer rich domains, and the void-rich domains, where the boundary surface is defined as the same manner that was adopted in Figure 4. We observe that the simulation results confirm the theoretical predictions.

It should be noted that the lattice discretization used in the simulations may affect the domain morphology. For example, the surfaces of the B-polymer in the case III (Figure 8, parts d−f), are almost flat although they are expected to be convex to the air phase. Same is true for the surfaces between polymer rich domains and the void rich domains in case II (Figure 8, parts a−c). If we use much finer lattice discretization, slightly convex structures would be realized. Apart from these discrepancies which arise from the numerical discretization, the DDF simulations reproduce the same structures of the free surface as those predicted by the theoretical phase diagrams. Thus we can conclude that the equilibrium balance of the interfacial tension is an important factor in deciding the structure of the free surface of the thin films.

5.2. Dependence of the Free Surface Structures on the Chain Length. In the construction of the phase diagrams shown in Figures 6 and 7, we fixed the chain lengths of the polymers A and B. Here, we study the dependence of the structures of the free surface on the chain lengths. Parts a and b of Figure 9 show the phase diagrams of free surface structures for the cases $N_A = N_B = 10$ and $N_A = N_B =$ infinity, respectively. Comparing them with Figure 6 ($N_A = N_B = 5$), we notice that the boundary of the region defined by eq 9 is shifted to the lower left, and those for eqs 10−12 are shifted to the lower side. These shifts are due to the correction terms in eqs 13−15 that have the $1/N$ dependence on the chan length N.

In Figures 6 ($N_A = N_B = 5$) and 9a ($N_A = N_B = 10$), the open circles indicate the parameter sets for which the sample simulations have been performed. From these phase diagrams, we predict that the system changes from the case II to the case III when both N_A and N_B are increased. Thus, shortening chains suppresses the surface roughening. (Multiblock grafted chains could also eliminate such a roughening, as we could easily check in the future work.) To check this prediction, we performed simulation using the same parameters as those shown in Figure 8a−c only changing the parameters $N_A = N_B = 5$ to $N_A = N_B = 10$, and the result is shown in Figure 10. It is seen that the surface roughening is taking place in this case, supporting the theoretical prediction.

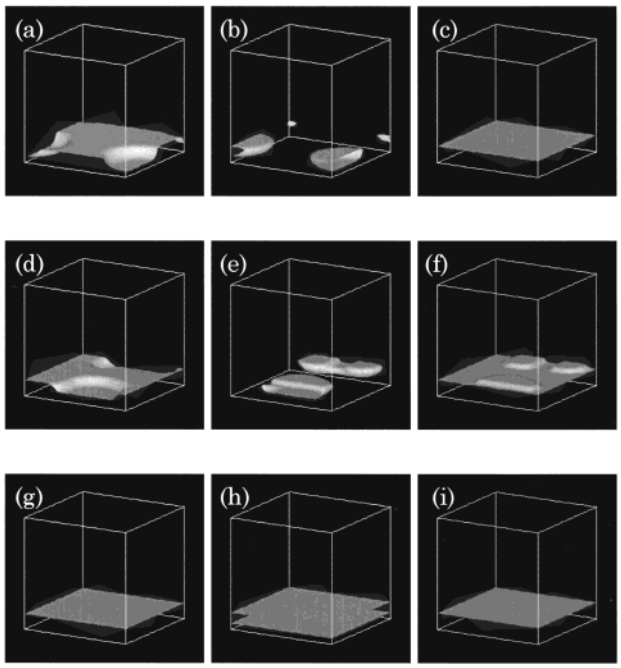

Figure 8. Simulation results of the domain boundaries of the phases rich in polymers A, B, and void at $t = 2500$. Parts a−c, d−f, and g−i show the structures calculated for the regions II, III, and IV in the phase diagram, respectively. Parts a, d, and g show the domain boundaries of polymer A, parts b, e, and h those of polymer B, and parts c, f, and i those of the void.

6. Concluding Remarks

We made an analysis of the surface structures of thin polymer blend films, where the phase separation takes place. To model such thin films, we introduced the effects of the substrate wall and of the boundary between the polymer phase and the air phase (the free surface). We obtained three types of phase separation, i.e., a layered structure near the substrate wall, a

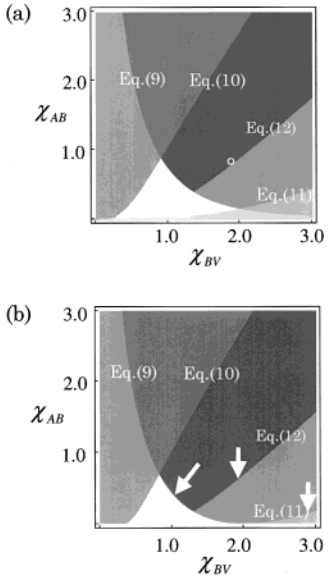

Figure 9. Phase diagrams for the surface roughening in the cases of (a) $N_A = N_B = 10$ and (b) $N_A = N_B =$ infinity with $\chi_{AV} = 2.0$, respectively. The definitions of the phase boundaries are the same as those in Figure 6. The open circle in part a corresponds to the open circle in Figure 6.

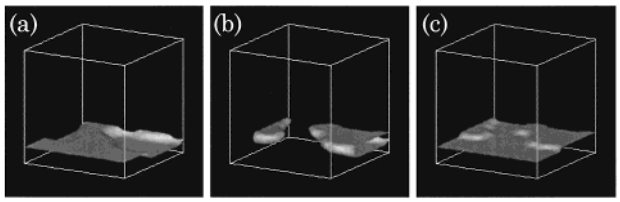

Figure 10. Same as Figure 8a−c but for $N_A = N_B = 10$. Part a shows the boundaries of the polymer A domains, part b that of the polymer B domains, and part c that of the void domains.

similar layered structure near the free surface, and a disoriented domain structure in the middle of the film. As the time evolves, the boundaries of the phase separated regions near the substrate wall and near the free surface propagate toward the center of the film. This phenomenon can be identified with the spinodal wave observed in the experiments.

We also observed a transient surface roughening structures. These surface roughening phenomena were explained using a simple theoretical model, where we assumed that the surface roughening is caused by the creation of droplets composed of the minority phase at the free surface. On the basis of this assumption, we considered the balance among the interfacial tensions using Neumann's triangle method. Using this equilibrium calculation, several structures are predicted as are summarized in Table 1. Furthermore, by substituting the approximated expressions for the interfacial tension, the above conditions are rewritten using 5 parameters, i.e. the χ parameters χ_{AB}, χ_{AV}, and χ_{BV} and polymer chain lengths N_A and N_B assuming $N_V = 1$, with which we can construct phase diagrams for the surface roughening.

To verify these theoretical phase diagrams, we performed dynamic density functional simulations, and confirmed that the obtained structures are consistent with the theoretical phase diagram. This means that the balance among the interfacial tensions at the free surface is one of the most important factors in determining the free surface structure. As it is easy to construct such a theoretical phase diagram, the method we proposed here will be a useful tool in predicting the surface structures.

Acknowledgment. The authors would like to thank T. Nishi, A. Takahara, T. P. Russell, J. Klein, T. Kerle, K. Tanaka, S. Kimura, H. Chawanya, Y. Makita, and the members of the Doi project for many helpful comments and discussions. This work is supported by the national project, which has been entrusted to the Japan Chemical Innovation Institute (JCII) by the New Energy and Industrial Technology Development Organization (NEDO) under METI's Program for the Scientific Technology Development for Industries that Create New Industries. This work is in part supported by the Scientific Research Fund of the Ministry of Science, Sports, and Culture, Japan.

References and Notes

(1) Yoshimura, T.; Shiraishi, H.; Yamamoto, J.; Okazaki, S. *Jpn. J. Appl. Phys.* **1993**, *32*, 6065.
(2) Tanaka, K.; Yoon, J.-S.; Takahara, A.; Kajiyama, T. *Macromolecules* **1995**, *28*, 934.
(3) Kajiyama, T.; Tanaka, K.; Ge, S.-R.; Takahara, A. *Prog. Surf. Sci.* **1996**, *52*, 1.
(4) Karim, A.; Slawecki, T. M.; Kumar, S. K.; Douglas, J. F.; Satija, S. K.; Han, C. C.; Russell, T. P.; Liu, Y.; Overney, R.; Sokolov, J.; Rafailovich, M. H. *Macromolecules* **1998**, *31*, 857.
(5) Krausch, G.; Dai, C. A.; Kramer, E. J.; Marko, J. F.; Bates, F. S. *Macromolecules* **1993**, *26*, 5566.
(6) Geoghegan, M.; Jones, R. A.; Clough, A. S. *J. Chem. Phys.* **1995**, *103*, 2721.
(7) Brown, G.; Chakrabarti, A. *Phys. Rev. A* **1992**, *46*, 4829.
(8) Puri, S.; Frisch, H. L. *J. Phys. Condens. Matt.* **1997**, *9*, 2109.
(9) Keilhorn L.; Muthukumar, M. *J. Chem. Phys.* **1999**, *111*, 2259.
(10) Karim A.; Douglas J. F.; Lee B. P.; Glotzer S. C.; Rogers J. A.; Jackman R. J.; Amis E. J.; Whitesides G. M. *Phys. Rev. E* **1998**, *57*, R6273.
(11) Fraaije, J. G. E. M. *J. Chem. Phys.* **1993**, *99*, 9202.
(12) Hasegawa, R.; Doi, M. *Macromolecules* **1997**, *30*, 3086.
(13) Zvelindovsky, A. V.; Sevink, G. J. A.; van Vlimmeren, B. A. C.; Maurits, N. M.; Fraaije, J. G. E. M. *Phys. Rev. E* **1998**, *57*, R4879.
(14) Matsen, M. W. *J. Chem. Phys.* **1997**, *106*, 7781.
(15) Pickett, G. T.; Balazs, A. C. *Macromol. Theory Simul.* **1998**, *7*, 249.
(16) Helfand, E.; Wasserman, Z. R. *Macromolecules* **1976**, *9*, 879.
(17) Hong, K. M.; Noolandi, J. *Macromolecules* **1981**, *14*, 727.
(18) Fleer, G. J.; Cohen Stuart, M. A.; Scheutjens, J. M. H. M.; Cosgrove, T.; Vincent, B. *Polymers at Interfaces*; Chapman & Hall: London, 1993.
(19) Hariharan, A.; Kumar, S. K.; Russell, T. P. *J. Chem. Phys.* **1993**, *98*, 6516.
(20) Theodorou, D. N. *Macromolecules* **1989**, *22*, 4578.
(21) DiMarzio, E. A. *J. Chem. Phys.* **1965**, *42*, 2101.
(22) Wu, S. *Polymer Interface and Adhesion*; Marcel Dekker: New York, 1982.
(23) Broseta, D.; Fredrickson, G. H.; Helfand, E.; Leibler, L. *Macromolecules* **1990**, *23*, 132.
(24) Yeung, C.; Balazs, A. C.; Jasnow, D. *Macromolecules* **1993**, *26*, 1914.
(25) Morita, H.; Kawakatsu, T.; Doi, M. Manuscript in preparation.

MA010346+